Large-Eddy Simulation of a Multi-Element LOx/CH$_4$ Thrust Chamber Demonstrator of a Liquid Rocket Engine

Christoph Traxinger, Julian Zips and Michael Pfitzner*
Institute for Thermodynamics, Bundeswehr University Munich
Werner-Heisenberg-Weg 39, 85577 Neubiberg, Germany

Abstract

The present study is concerned with the numerical investigation of a thrust chamber demonstrator (TCD) mimicking a main stage engine. The focus is put on the combustion process and the flame-flame interaction. Two different topics are addressed: First, the influence of recess and tapering is assessed by means of a single-element configuration. Second, a 60 degrees section of the TCD's combustion chamber is simulated where 15 injection elements are fully resolved. The results show, that flame-flame interaction significantly affects the combustion process and results in a very different flow field compared to the single-element case.

1. Introduction

The most promising propellant combination for future reusable liquid-propellant rocket engines (LREs) is methane (CH$_4$) and liquid oxygen (LOx), see, e.g., Zurbach et al.[29] or Preclik et al.[16] The main reason for the intensified interest in LOx/CH$_4$ is the demand for significantly lower costs for bringing cargo into space especially since private companies have entered the market. The advantages from using methane as LRE-fuel are diverse: In contrast to LOx/hydrogen(H$_2$), which is commonly used in nowadays rocket engines, e.g., Vulcain or Vinci, methane has the benefit of low production and handling costs and is furthermore easier to store. In addition, methane tanks can be designed much smaller compared to hydrogen tanks, which results in an overall lighter design of the rocket giving the opportunity to transport a heavier payload into space. Due to the similarity of methane and oxygen with respect to the critical point and the density, the bulkhead design and the turbopumps get much simpler compared to common LOx/H$_2$ configurations. One of the disadvantages of methane compared to hydrogen is the smaller specific impulse. However, compared to kerosene the specific impulse created with methane is still higher.

Although the discussion of methane as future fuel is not quite new and is present for more than a decade, there is still a lack of knowledge regarding high-pressure O$_2$/CH$_4$ combustion. Furthermore, since reusability is one of the future trends for significantly lowering the costs, the accurate prediction of thermal loads is an essential component of the development process of methane fired LREs. A promising tool to gain further insight and knowledge about relevant physical phenomena in high-pressure O$_2$/CH$_4$ combustion is Large-Eddy Simulation (LES). An important step in the development of such numerical tools are appropriate validation cases with well-reported operating and boundary conditions in order to gain confidence in the applied methods.

In recent years, two different methane-fired sub-scale combustion chambers have been investigated by means of experiments at the Technical University of Munich. Both chambers are operated under ideal-gas conditions and validation data for numerical tools is provided in terms of chamber pressure profiles and wall heat fluxes. One combustion chamber is a single-element configuration with a capacitive cooling, see Celano et al.[2] The other one is a 7-element sub-scale combustion chamber which is cooled by a water jacket, see Silvestri et al.[20] Different groups[4, 6, 9, 10, 12, 17, 18] have investigated theses two sub-scale combustors and validated their tools. In our two most recent publications,[27, 28] we also used these two test cases[2, 20] and found a good agreement between the numerical and experimental results. Regarding LRE-like methane combustion, i.e., liquid-like injection of the oxidizer, the test case G02[21] conducted at the Mascotte test bench is very popular for numerical validation. Many different numerical groups have successfully simulated this case including two recent studies from our group.[24, 26]

---

*Corresponding author: christoph.traxinger@unibw.de

LES OF A MULTI-ELEMENT LOX/CH$_4$ THRUST CHAMBER DEMONSTRATOR OF AN LRE

Building on the successful validation of our simulation tools, we started working on the numerical investigation of an application-relevant full-scale LOx/CH$_4$ thrust chamber demonstrator (TCD) mimicking a main stage engine of the 1000 kN thrust class. The TCD was defined by ArianeGroup within the framework of the SFB/TRR 40. It represents a future reusable LRE and is inspired by the Prometheus engine. In the current work, we present first results of the conducted numerical simulations. Up to now, an adiabatic combustion model is applied and therefore the focus lies on the investigation of the combustion process and related phenomena.

The paper is structured as follows: In the next section, the investigated thrust chamber demonstrator is described. After that, the numerical setup and modeling is introduced in Sec. 3. The results of the simulations are presented in Sec. 4. Finally, in Sec. 5 conclusions are drawn and an outlook for future work is given.

2. Description of the Investigated Thrust Chamber Demonstrator

The thrust chamber demonstrator (TCD) defined by ArianeGroup is operated at a combustion chamber pressure p_{cc} of 100 bar and is mainly inspired by the operating conditions of the Prometheus engine. Typical injection conditions for both oxidizer and fuel are used: O$_2$ is injected at subcritical temperature and supercritical pressure, i.e., in a liquid-like state. As the engine is cooled using a regenerative circuit, CH$_4$ enters the combustion chamber in a gas-like state, i.e., both temperature and pressure are supercritical. Table 1 and Fig. 1 summarize the injection conditions. According to Tab. 1, the oxidizer-fuel ratio (ROF) amounts 3.4 which results in a fully burned state lying below the stoichiometry.
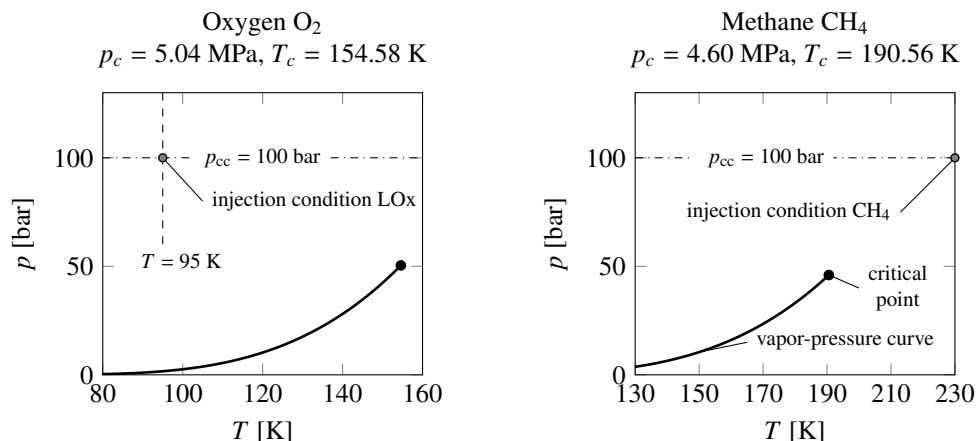
Figure 1: Visualization of the injection conditions in the appropriate pressure-temperature diagrams of O$_2$ (left) and CH$_4$ (right). The solid line represents the vapor pressure curve which is determined at the critical point.

In Fig. 2 the geometry of the injector head and the contour of the combustion chamber up to the throat is shown. The injector head has a diameter of 400 mm and features 12 rows of injection elements in radial direction. Six coaxial injection elements are installed at the inner row at a radius of r = 15.75 mm. In each row following the first one six additional elements are added and therefore the outermost row (r = 189 mm) comprises 72 injection elements. In total, the injector head features 468 elements. In Fig. 3 left a detailed drawing of a single injection element is shown. The methane annulus and the posttip have a height of 0.5 mm and 0.45 mm, respectively. The original injection element features a recess of 4 mm as well as a tapering with an angle of eight degrees in order to increase the mixing of fuel and oxidizer and thereby reduce the required chamber length for guaranteeing complete combustion.

Table 1: Injection conditions for the investigated TCD. The nominal combustion chamber pressure is p_{cc} = 100 bar.

	O$_2$	CH$_4$
Temperature [K]	95	230
Density [kg/m^3]	1189.1	143.3
Mass flow rate [g/s]	461.9	135.9
Velocity [m/s]	12.46	78.41
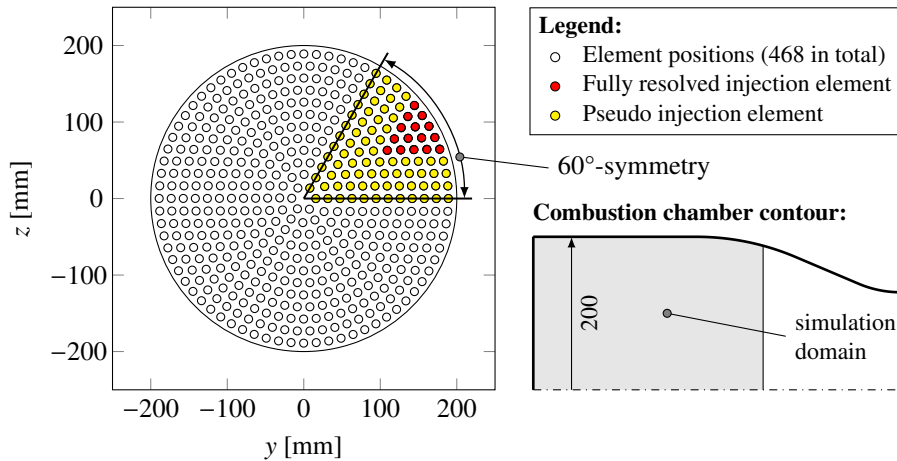
Figure 2: Geometry of the investigated TCD.

3. Numerical Setup

3.1 Simulation Domain and Mesh Topology

According to Fig. 2, several simplifications have been made to arrive at a manageable grid: First of all, the symmetry of the injector head was used and therefore a 60 degrees section has been considered, see Fig. 2 left. In this way, cyclic boundary conditions are applied and the number of injection elements represented in the LES reduces to 78. Next, as we are interested in the flame-flame and the flame-wall interaction and in future work in the prediction of the wall heat flux and the local thermal load, we decided to fully resolve 15 injector elements in the near-wall region. The resolved injectors are marked in red in Fig. 2 left. The resolved injection elements have been mapped onto the faceplate and a local mesh refinement strategy was used to properly resolve the elements on the faceplate and the combustion process further downstream, see Fig. 4 right. Therefore, we get a high-quality grid with hexahedral cells and can refine the mesh in the regions of interest, i.e., properly resolve the flow field under the present high-pressure conditions. The mapping of the injection elements implies a simplification of its actual geometry, namely the neglection of the recess and the tapering, see Fig. 3. In Subsec. 4.2 we discuss the effects of this simplification for a single-element

a) Original.   b) Simplification.
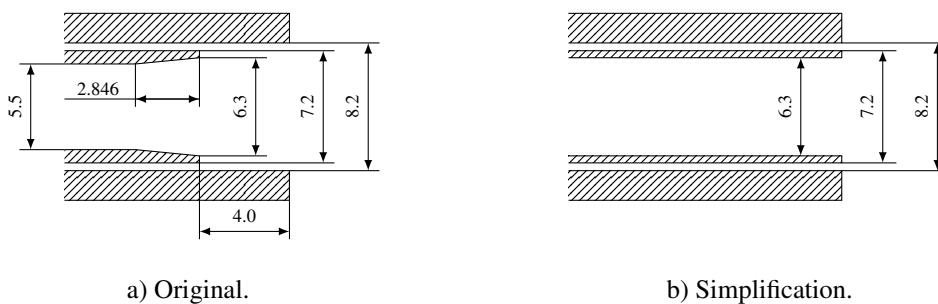
Figure 3: Dimensions of a single injection element: a) Original configuration with tapering and recess; b) Flush-mounted simplification as it is applied in the present LES of the TCD.

configuration. The remaining injection elements, namely 51 full and 24 half elements, have been modeled as pseudo injection elements. This means that a single-hole inlet has been mapped onto the faceplate with the outer diameter of the methane annulus, i.e., 8.2 mm. A fully-burned (fb) mixture is injected through the pseudo injection elements. For the present ROF of 3.4 this results in a mixture fraction of $f_{fb} = 0.227$ at a temperature and density of 3632.7 K and 7.87 kg/m³, respectively. The velocity was determined based on the density, total mass flux and the area occupied by the injector head and amounts 282.89 m/s.

Finally, we decided to truncate the combustion chamber after 300 mm, see Fig. 2 right, which is sufficient to investigate the injection, mixing and combustion processes. In the present study, the posttip is radially resolved with seven cells. This results in the total grid size of 85 million cells. Figure 4 gives an overview over the applied simulation domain and shows the mesh resolution in the region of the resolved injection elements.

LES OF A MULTI-ELEMENT LOX/CH₄ THRUST CHAMBER DEMONSTRATOR OF AN LRE
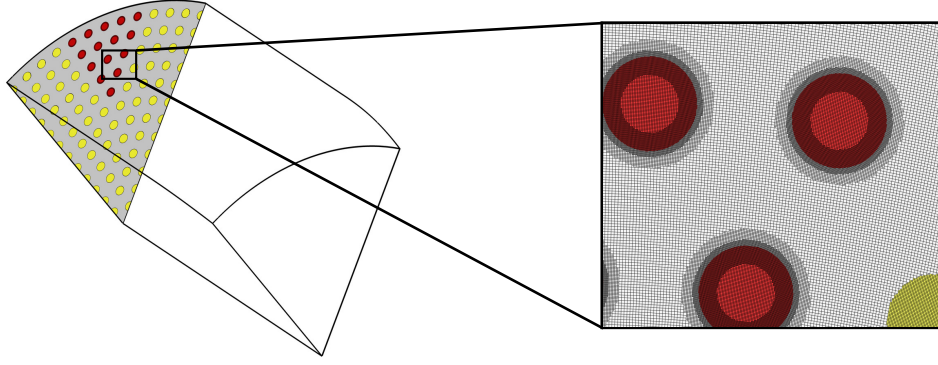
Figure 4: Overview of the simulation domain and the local refinement in the region of the injection elements.

3.2 Governing Equations

Large Eddy Simulations were conducted using a pressure-based version of OpenFOAM based on the Favre-filtered conservation equations of mass

$$\partial_t \bar{\rho} + \nabla \cdot (\bar{\rho} \tilde{\mathbf{u}}) = 0 \tag{1}$$

and momentum

$$\partial_t \bar{\rho} \tilde{\mathbf{u}} + \nabla \cdot (\bar{\rho} \tilde{\mathbf{u}} \tilde{\mathbf{u}}) = -\nabla \bar{p} + \nabla \cdot \bar{\tau} + \nabla \cdot \tau^{\mathrm{sgs}} \; . \tag{2}$$

Here, ρ, $\mathbf{u}$ and p are the density, velocity vector and pressure, respectively. In addition, the superscript sgs denotes the unresolved sub-grid scale contributions resulting from the applied Favre filtering. The operators ∂_t and ∇ are the time and spatial derivatives, respectively. For Newtonian fluids, the hypothesis of Stokes together with the gradient diffusion hypothesis[15] are applied. The elements of the strain rate tensor can hence be calculated as:

$$\bar{\tau}_{ij} + \tau_{ij}^{\mathrm{sgs}} = 2 \left(\bar{\mu} + \mu^{\mathrm{sgs}} \right) \left(\overline{S}_{ij} - \frac{1}{3} \overline{S}_{kk} \delta_{ij} \right) \tag{3}$$

with

$$\overline{S}_{ij} = \frac{1}{2} \left(\frac{\partial \tilde{u}_i}{\partial x_j} + \frac{\partial \tilde{u}_j}{\partial x_i} \right) \; . \tag{4}$$

In Eq. (3), μ denotes the laminar and μ^{sgs} the eddy viscosity which is determined using the Vreman sgs model.[25] δ_{ij} is the Kronecker delta. For convenience, the Newtonian notation is chosen for the deformation tensor in Eq. (4).

To model the combustion process, a tabulation approach is applied. This is motivated by the fact that hydrocarbon combustion involves a large number of species and reactions which would result in large computational costs when solved during run-time. Under the assumption of adiabatic combustion, the species and energy conservation equations are replaced by a transport equation for the mixture fraction f:

$$\partial_t \bar{\rho} \tilde{f} + \nabla \cdot \left(\bar{\rho} \tilde{\mathbf{u}} \tilde{f} \right) = \nabla \cdot \left(\frac{\bar{\mu}}{Sc} + \frac{\mu^{\mathrm{sgs}}}{Sc_t} \right) \nabla \tilde{f} \; . \tag{5}$$

According to Cabrit and Nicoud,[1] the turbulent Schmidt number Sc_t was set to 0.7. The same was done for the laminar Schmidt number Sc in the present study. In order to describe unresolved fluctuations of mixture fraction, we solve a transport equation for its variance given by Kemenov et al.[8]

$$\partial_t \bar{\rho} \widetilde{f''^2} + \nabla \cdot \left(\bar{\rho} \tilde{\mathbf{u}} \widetilde{f''^2} \right) = \nabla \cdot \left(\frac{\bar{\mu}}{Sc} + \frac{\mu^{\mathrm{sgs}}}{Sc_t} \right) \nabla \widetilde{f''^2} - 2 \bar{\rho} \tilde{\chi} + 2 \left(\frac{\bar{\mu}}{Sc} + \frac{\mu^{\mathrm{sgs}}}{Sc_t} \right) \left(\nabla \tilde{f} \right)^2 \; . \tag{6}$$

Here, χ denotes the scalar dissipation rate which is modeled according to Domingo et al.[5] as the sum of the resolved and the sgs contributions:

$$2 \bar{\rho} \tilde{\chi} = 2 \frac{\bar{\mu}}{Sc} \left(\nabla \tilde{f} \right)^2 + C_\chi \frac{\mu^{\mathrm{sgs}}}{Sc_t} \frac{\widetilde{f''^2}}{\Delta^2} \; . \tag{7}$$

The model constant C_χ is set to 2 according to Kemenov et al.[8] Δ represents the local filter width which is classically determined as the cube root of the cell volume.

For building-up the thermo-chemical tabulation, the flamelet concept originally derived by Peters[13] is used. Assuming that the chemical time scales are smaller than the turbulent time scales, a turbulent non-premixed flame can be represented by a brush of laminar counterflow diffusion flames. In an axisymmetric configuration, the governing equations reduce to a one-dimensional problem that can be solved in mixture fraction space f. Under the assumption of a unitary Lewis number for all species ($Le_i = Le = 1$), the so-called flamelet equations read:[13]

$$\rho\, \partial_t\, Y_i = \rho \frac{\chi}{2} \frac{\partial^2 Y_i}{\partial f^2} + \dot{S}_i \,, \tag{8}$$

$$\rho\, \partial_t\, h = \rho \frac{\chi}{2} \frac{\partial^2 h}{\partial f^2} \,. \tag{9}$$

Here, h denotes the absolute enthalpy. In addition, Y_i and $\dot{S}_i$ are the mass fraction and chemical source term of species i, respectively. The GRI-3.0[7] mechanism is used in the present study to determine $\dot{S}_i$. The mechanism involves 53 species and 325 reactions. The scalar dissipation rate χ in Eqs. (8) and (9) is modeled according to Peters[13] as $\chi = \chi_{st} \exp(-2[\mathrm{erfc}^{-1}(2f)]^2)$, where χ_{st} denotes the scalar dissipation rate at stoichiometry.

For the present study, the thermo-chemical database for the LES consists of $1011 \times 10 \times 13 \times 25$ points in $\widetilde{f}, \widetilde{f''^2}$, $\widetilde{\chi}_{st}$ and $\bar{p}$. The maximum scalar dissipation rate amounts $\widetilde{\chi}_{st,max} = 500000$ s^{-1}. Statistical independence of the thermo-chemical parameters is assumed, i.e., $\mathcal{P}(f, \chi_{st}, p) = \mathcal{P}(f)\mathcal{P}(\chi_{st})\mathcal{P}(p)$. For the generation of the tabulation approach, presumed probability density functions (PDFs) are used to calculate the filtered variables. For the mixture fraction a β-shaped PDF and for both the scalar dissipation rate as well as the pressure Dirac functions are applied. For further details on the flamelet and table generation see Zips et al.[26] Details regarding the solver and the overall numerical framework can be found in, e.g., Müller et al.[11] or Traxinger et al.[23]

3.3 Thermodynamics Model

For closing the above system of governing equations, the Soave, Redlich and Kwong[22] (SRK) cubic equation of state (EOS) is applied in this study:

$$p = \frac{\mathcal{R}\, T}{v - b} - \frac{a}{v^2 + bv} \,. \tag{10}$$

Here, v and $\mathcal{R}$ denote the molar volume and the universal gas constant, respectively. The cubic EOS takes into account both attractive and repulsive forces by means of the parameters a and b, respectively, and is therefore able to model the liquid-like injection conditions occurring in LREs. A discussion of its accuracy can be found in, for instance, one of our recent publications, see, e.g., Traxinger et al.[24] For linking the thermal EOS with the calorical properties like, e.g., enthalpy h, the departure function formalism is applied, cf. Poling et al.[14] Suitable mixing rules[19] are used to describe the multicomponent mixture. The visocsity is modeled according to the approach of Chung et al.[3]

4. Results

4.1 Counterflow Diffusion Flame

In Fig. 5 the results of the nominal flamelet at the investigated operating conditions, see Tab. 1, in terms of the temperature and the density are shown. The maximum temperature occurs around the stoichiometric mixture fraction $f_{st} = 0.2$
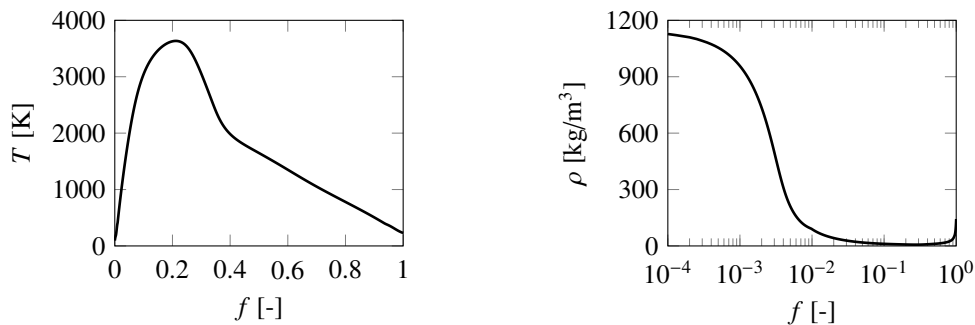
Figure 5: Temperature and density variation across the flamelet at the nominal operating conditions, see Tab. 1, and for a scalar dissipation rate of $\chi_{st} = 1$ s^{-1}.
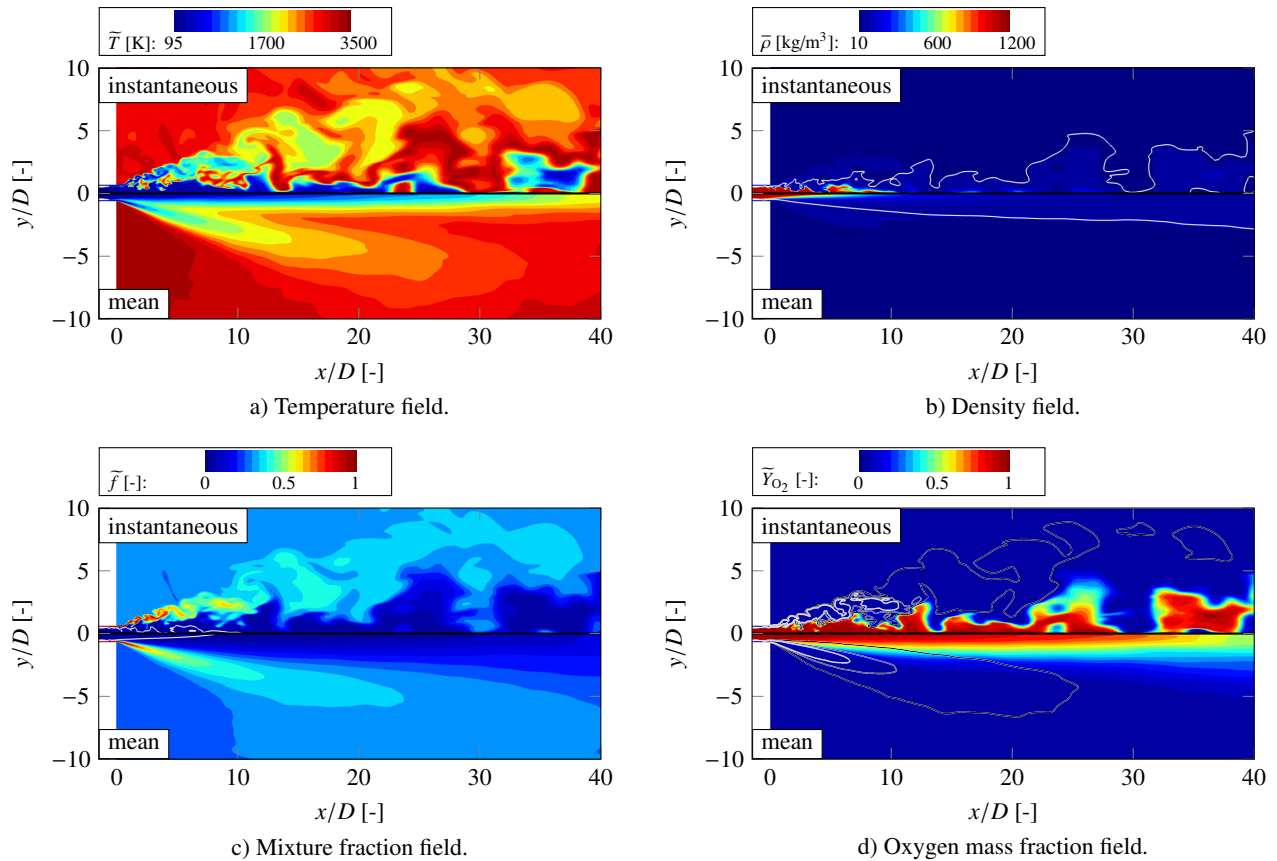
Figure 6: Overview of the reacting flow field for the original configuration. The white line in b) corresponds to the stoichiometric mixture fraction $f_{st} = 0.2$. In c) the white line marks the pseudo-boiling point which at an pressure of 100 bar corresponds to a density of 488.9 kg/m^3. In d) iso-contours of the methane mass fraction are highlighted by the solid lines corresponding to $Y_{CH_4} = [0.2, 0.1, 0.01]$.

and amounts to approximately 3500 K. To the left of the stoichiometric point, i.e., $f < 0.2$, a steep temperature gradient is present at the oxidizer-rich side. This strong increase comes along with a large variation in density caused by the transcritical injection process, i.e., the transition from a high to a low density state, see Fig. 5 right. Note the logarithmic scaling of the abscissa in the density plot. To the right of the stoichiometric point, i.e., $f > 0.2$, a typical diffusion flame structure is observed. In a recent study, Maestro et al.[10] applied a finite rate approach for the single-element GOx/GCH$_4$ test case of Celano et al.[2] The comparison of their LES scatter data with laminar counterflow diffusion flames encourage the application of a flamelet-based combustion model.

4.2 Assessment of the Injection Element Modeling

In order to evaluate the influence of the simplified injection element modeling in LES of the TCD, i.e., the mapping of the injector onto the faceplate, single-element simulations have been conducted for the original geometry, compare Fig. 3a, and the simplification, see Fig. 3b. The posttip is radially resolved with 15 cells and the length of the domain corresponds to the length of the simulated TCD configuration, i.e., 300 mm.

In Fig. 6 the reacting flow field downstream of the original injector configuration up to an axial position of $x/D = 40$ is shown by means of instantaneous snapshots and plots of the averaged flow field. A very thin and highly turbulent flame is emanating from the injector. As a result of the shear forces, large-scale structures are forming quickly downstream of the faceplate which can be seen in terms of the instantaneous temperature plot in Fig. 6a top. In the mean temperature field, the influence of the sgs turbulence modeling can be comprehended as the temperature in the flame region clearly falls below the adiabatic flame temperature of approximately 3500 K. The highly turbulent flow field leads to a quick fragmentation of the dense oxygen core starting already downstream of $x/D \approx 2$. This process can

be seen in more detail in terms of the density field shown in Fig. 6b, which gets strongly disrupted by the strong shear forces. The white line in Fig. 6b corresponds to the stoichiometric mixture fraction of $f_{st} = 0.2$ and marks the position of the flame. As a result of the rather weak mixing, the flame does not close towards the end of the domain which can be seen in terms of the averaged flow field in Fig. 6b bottom. In addition, methane is consumed very rapidly, see Fig. 6c, and an oxygen-rich mixture is present downstream of $x/D \geq 15$. Large methane mass fractions of $Y_{CH_4} \geq 0.2$ can only be found up to an axial position of $x/D \approx 10$. This is highlighted in Fig. 6d by means of methane iso-contours superimposed onto the oxygen mass fraction field. Based on Fig. 6d, the highly turbulent and fragmented flow field can be comprehended again in terms of the instantaneous oxygen mass fraction field.

In Fig. 7 the results of the original and the simplified configuration are compared to each other by means of the instantaneous (left column) and the time-averaged (right column) flow field. As already discussed above, both injector configurations show a highly turbulent and thin flame downstream of the injection element. Due to the plain mapping of the simplified configuration, the break-up process and the development of large-scale turbulence takes longer. This can be seen in a smaller spreading angle of the total flow field marked by the dash-dotted line in Fig. 7a. Whilst the original configuration shows an angle of approximately 30 degrees, the analysis of the simplified configuration reveals an angle of approximately 24 degrees. This fact can also bee seen in the averaged temperature fields shown in Fig. 7b.

a) Instantaneous temperature field.

b) Mean temperature field.

c) Instantaneous density field.

d) Mean density field.
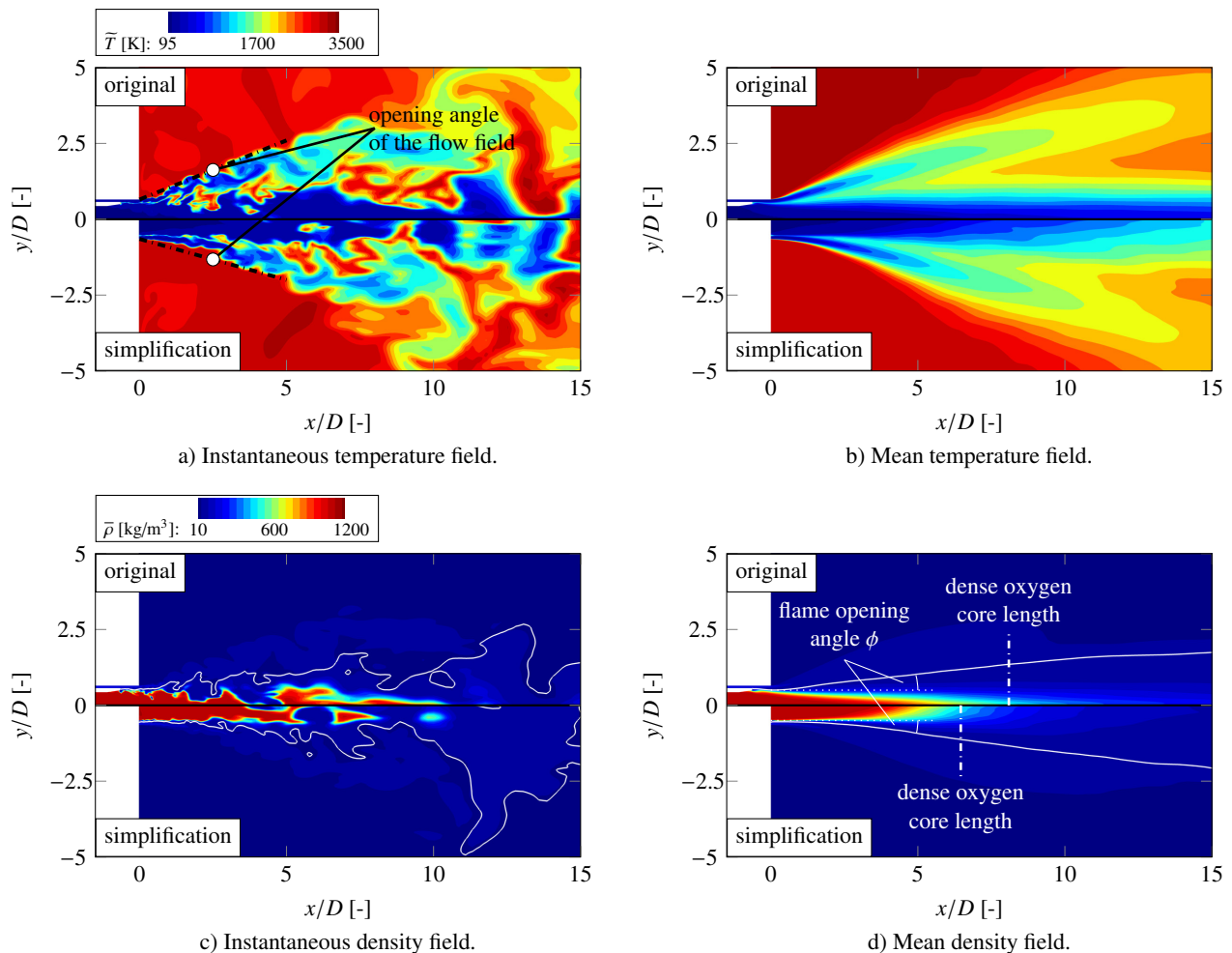
Figure 7: Qualitative comparison between the original and the simplified configurations. The dash-dotted line in a) marks the qualitative opening angle of the total flow field. In c) and d) the white lines corresponds to the stoichiometric mixture fraction $f_{st} = 0.2$. In addition, the dense oxygen core length and the flame opening angle are marked in d).

The slower development of turbulent structures with respect to the axial position can be underlined by the reduced fragmentation of the dense oxygen core in the simplified configuration, see Fig. 7c bottom. Here, only packages of dense oxygen detach at around $x/D = 5$, but upstream the turbulence acting on the dense oxidizer core is not strong enough to break-up the structure like in the case of the original configuration, see Fig. 7c top. These differences in the

LES OF A MULTI-ELEMENT LOX/CH$_4$ THRUST CHAMBER DEMONSTRATOR OF AN LRE

flow topology result in different lengths of the dense oxygen core in the averaged flow field which are marked in Fig. 7d by the dash-dotted white lines. The length of the oxygen core was defined with the help of the pseudo-boiling (pb) point which corresponds for 100 bar to a density value of 488.9 kg/m^3. In addition, Fig. 7d shows the flame opening angle ϕ which was defined by means of the radial extent of the stoichiometric mixture fraction at $x/D = 5$. For the original configuration (index: o) this yields an angle of $\phi_\mathrm{o} = 11.8°$ and for the simplified configuration (index: s) the flame opening angle is slightly smaller corresponding to $\phi_\mathrm{s} = 10.6°$.

Going more into detail, the change in density, oxygen mass fraction and temperature along the chamber axis up to $x/D = 40$ is plotted in Fig. 8. Due to the liquid-like injection of the oxidizer, a large density stratification is present, see Fig. 8a. The spatial gradient of the density along the center axis of the chamber is different for both configurations resulting in varying locations of the pseudo-boiling point, compare Fig. 7d. Slightly upstream of the pseudo-boiling point, the largest density fluctuations occur, see Fig. 8d. In case of the simplified configuration, the transition from the liquid-like (high) density state to the gas-like (low) density state takes place in a very narrow region, which gets obvious in both the average and the RMS values of the density. In contrast, the transition within the original injector configuration stretches over a broader region along the chamber axis. This fact can be further underlined by the change of the oxygen mass fraction. In the original configuration, 50% of the oxidizer are still present at $x/D = 40$ whereas in the simplified case, approximately 70% of the oxygen has been consumed up to this position. As a result, the RMS values for $x/D \leq 30$ are larger for the simplified case than for the original one. The slower transition process gets also visible in terms of the temperature change along the chamber axis, see Fig. 8c. For the simplified case the temperature gradient downstream of $x/D = 5$ is approximately 13 K/mm whereas for the original configuration the gradient amounts to approximately 8.5 K/mm. In terms of RMS temperature values, the findings for the oxygen mass fraction can be recalled, i.e., the fluctuations are larger for the simplified version for $x/D \leq 30$.
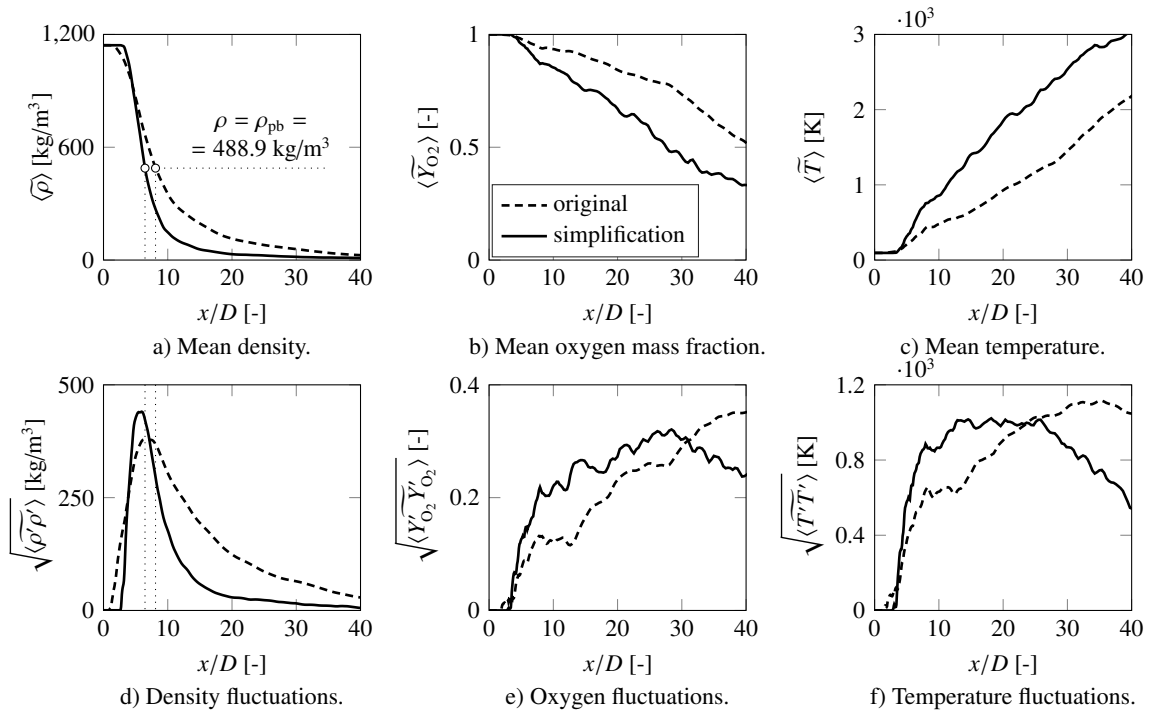
Figure 8: Influence of the injector modeling on the mixing and flame characteristic along the chamber axis ($0 \leq x/D \leq 40$) by means of averaged and RMS values.

4.3 Investigation of the Multi-Element TCD

In Fig. 9 the instantaneous and the average temperature field for the simulated multi-element TCD are shown. Five different planes are used to visualize the flames emanating from the injection elements, namely a single cut through the center of the simulation domain and four axial planes at $x/D = 10, 20, 30$ and 40. For visualization purpose, the faceplate and the injection elements are shown and colored according to Figs. 2 and 4. Looking at the instantaneous

a) Instantaneous temperature field. b) Mean temperature field.
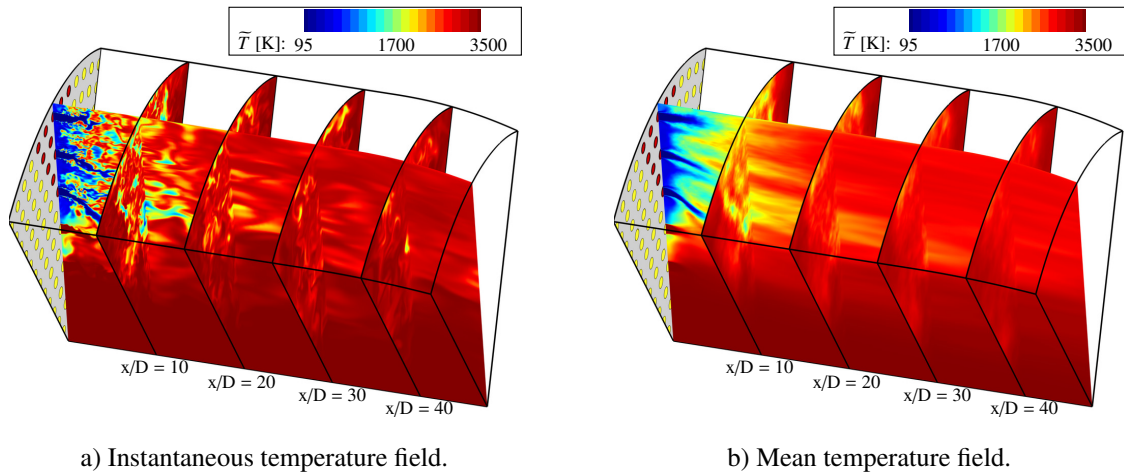
Figure 9: Instantaneous and averaged temperature fields in the TCD.

temperature field in Fig. 9a, a highly turbulent and disrupted flow field gets obvious. Thin flames are emanating from the injection elements and start to interact with each other downstream of $x/D \approx 3$. This leads to a quite different combustion process and overall flow field characteristics compared to the single-element configuration discussed in Subsec. 4.2. Temperatures below 1500 K are only present for $x/D \lessgtr 10$ which is true for both the instantaneous as well as the averaged temperature fields. In the single-element configuration, temperatures below 1500 K are present up to $x/D \approx 30$ in the mean temperature field. This is a result of the weak mixing process which is in the TCD case enhanced by flame-flame interaction. As it can be seen in Fig. 9b, the intensified mixing in the TCD leads to a sudden end of the low temperature zone ($T < 1500$ K) at $x/D \approx 5$. Another fact which becomes obvious when examining the TCD results is the bending of the middle and lower flames towards the center line of the combustion chamber. Due to the expansion of the surrounding flames and the low injection density through the pseudo injection elements, the outer flames expand towards regions of lower flow resistance. Therefore, we will later focus on the upper flame row at the outermost radius when investigating the flame structure and the combustion process in more detail.

In order to further characterize and understand the overall flame structure in the multi-element chamber, Fig. 10 shows the instantaneous and averaged mixture fraction fields. As a result of the strong flame-flame interaction, methane-rich mixtures ($f > 0.5$) are only present for $x/D \lessgtr 10$ which is very similar to the single-element configuration. However, due to the formation of a re-circulation zone – not present in the single-element case – fuel-rich gas is trapped in the region close to the faceplate. Downstream of $x/D = 10$, the mixture fraction is well below 0.5 and close to stoichiometry, i.e., close to the fully burned mixture having a mixture fraction of $f_{fb} = 0.227$.

a) Instantaneous mixture fraction field. b) Mean mixture fraction field.
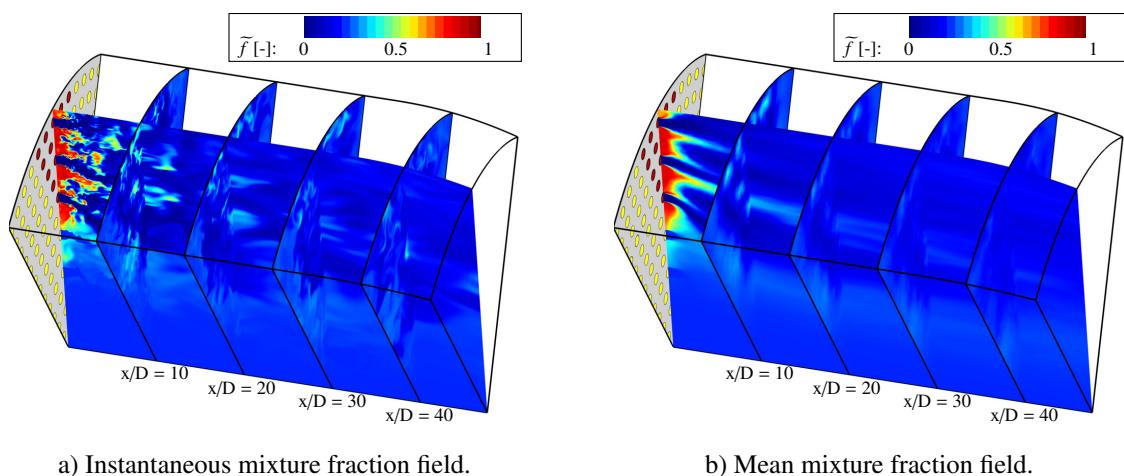
Figure 10: Instantaneous and averaged mixture fraction fields in the TCD.

9

LES OF A MULTI-ELEMENT LOX/CH$_4$ THRUST CHAMBER DEMONSTRATOR OF AN LRE

Figure 11 shows a cut at constant radial position through the injection elements of the outermost row, i.e., a radial cut through five resolved injector elements at $r = 189$ mm. Starting the observations in Fig. 11a, both the mean and the instantaneous temperature field again underline the pronounced flame-flame interaction and the resulting enhanced combustion process compared to the single-element case. The accelerated combustion process gets further obvious in the assessment of the dense oxygen core length, see Fig. 11b. Here, a length of $x/D \approx 3$ can be observed which is by more than a factor of two shorter than the length found in the single-element investigation, cf. Fig. 7b. Furthermore, due to the flame-flame interaction the shape of the dense oxygen core in the TCD more closely reassembles that found for the original single-element configuration, compare Fig. 7b upper half. Therefore, it is concluded that due to the strong flame-flame interaction the error introduced by the simplified injection element modeling is less pronounced in the multi-element case compared to the single-element case. Coming to the mixture faction field shown in Fig. 11c, the averaged field in the lower half shows the size of the re-circulation zone in both the circumferential and the axial direction. In the axial direction, the length approximately corresponds to the extent of the dense oxygen core. Downstream of this fuel-rich zone, methane is consumed quickly and the mixture tends towards the fully-burned state, i.e., $f_{fb} = 0.227$. Finally, Fig. 11d shows the oxygen mass fraction field. Here, the strong fragmentation of the flame and the oxygen core as well as the rapid combustion process can be comprehended again. In conclusion, the assessment of Figs. 9-11 shows that the main combustion process takes place at $x/D \lessgtr 10$ resulting from the strong flame-flame interaction.

a) Temperature field.

b) Density field.

c) Mixture fraction field.

d) Oxygen mass fraction field.
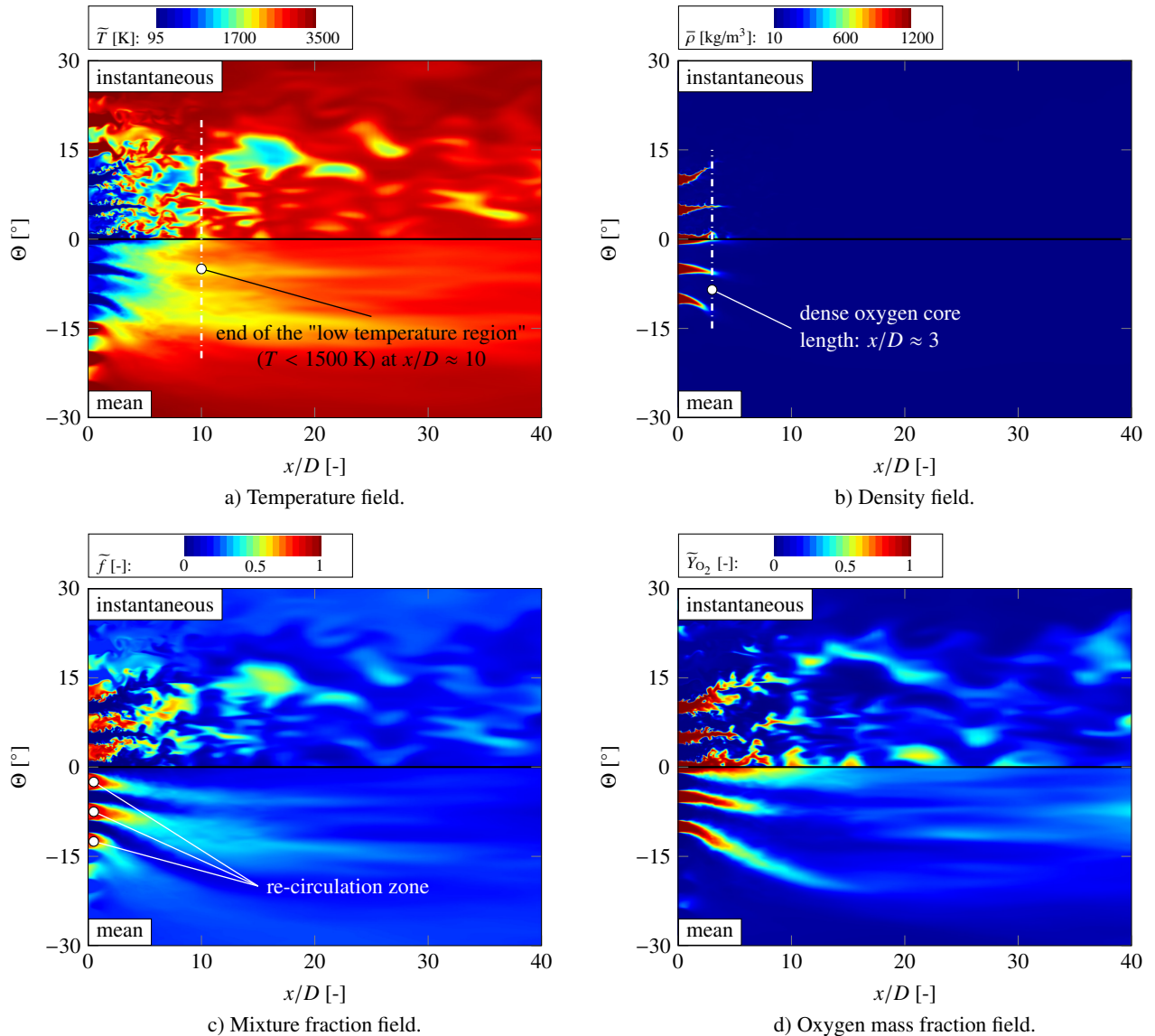
Figure 11: Overview of instantaneous and average flow field variables at the outermost injector row of the TCD shown by means of a cut at constant radial position. The angle in circumferential direction is denoted as Θ.

5. Conclusion and Outlook

For the cost-efficient production and operation of future reusable liquid rocket engines the propellant combination methane CH$_4$ and liquid oxygen LOx is very promising. In the present study, a LOx/CH$_4$ thrust chamber demonstrator (TCD) of the 1000 kN thrust class is examined by means of Large-Eddy Simulation (LES). The TCD is inspired by the Prometheus engine and was defined by ArianeGroup within the framework of the SFB/TRR 40. Two different topics have been addressed in the present investigation: First, the influence of recess and tapering was investigated by means of a single-element configuration. The comparison with a flush-mounted configuration showed that the two modifications have a noticeable influence on both the flame opening angle and the dense oxygen core length. Second, a 60 degrees section of the combustion chamber of the TCD was simulated. 15 injection elements in the near-wall region have been fully resolved. Due to the strong flame-flame interaction, an enhanced combustion process compared to the single-element case was found. As a result, large parts of the combustion take place at $x/D \lessgtr 10$ which is significantly shorter than in the investigated single-element configuration.

In future work, we are planning to focus on the flame-wall interaction and therefore on the prediction and investigation of wall heat fluxes and thermal loads. In this context, the application of a non-adiabatic flamelet model is mandatory and the accurate modeling of the near-wall flow will be an essential topic.

6. Acknowledgments

References

[1] O. Cabrit and F. Nicoud. Direct Simulations for Wall Modeling of Multicomponent Reacting Compressible Turbulent Flows. *Physics of Fluids*, 21:055108, 2009.

[2] M. P. Celano, S. Silvestri, G. Schlieben, C. Kirchberger, O. J. Haidn, and O. Knab. Injector Characterization for a Gaseous Oxygen-Methane Single Element Combustion Chamber. *Progress in Propulsion and Physics*, 8:145–164, 2016.

[3] T. Chung, M. Ajlan, L. Lee, and K. E. Starling. Generalized multiparameter correlation for nonpolar and polar fluid transport properties. *Ind. Eng. Chem. Res*, 27(4):671–679, 1988.

[4] Y. Daimon, H. Negishi, S. Silvestri, and O. Haidn. Conjugated combustion and heat transfer simulation for a 7 element gox/gch4 rocket combustor. In *54th AIAA/SAE/ASEE Joint Propulsion Conference and Energy Forum: AIAA paper 2018-4553*, 2018.

[5] P. Domingo, L. Vervisch, and D. Veynante. Large-Eddy Simulation of a Lifted Methane Jet Flame in a Vitiated Coflow. *Combustion and Flame*, 152:415–432, 2008.

[6] D. Eiringhaus, D. Rahn, H. Riedmann, O. Knab, and O. Haidn. Numerical investigation of a 7-element gox/gch4 subscale combustion chamber. In *Proceedings of the 7th European Conference for Aeronautics and Aerospace Sciences, Milano, Italy*, 2017.

[7] GRI-Mech 3.0. *http://www.me.berkeley.edu/gri mech*. University of California at Berkeley, 2000.

[8] K. A. Kemenov, H. Wang, and S. B. Pope. Modelling Effects of Subgrid-Scale Mixture Fraction Variance in LES of a Piloted Diffusion Flame. *Combustion Theory and Modelling*, 16(4):611–638, 2012.

[9] P. E. Lapenna, R. Amaduzzi, D. Durigon, G. Indelicato, F. Nasuti, and F. Creta. Simulation of a single-element gch4/gox rocket combustor using a non-adiabatic flamelet method. In *54th AIAA/SAE/ASEE Joint Propulsion Conference and Energy Forum: AIAA paper 2018-4872*, 2018.

[10] D. Maestro, B. Cuenot, L. Selle, G. Frank, M. Pfitzner, Y. Daimon, R. Keller, P. Gerlinger, A. Chemnitz, T. Sattelmayer, and O. Haidn. Numerical Investigation of Flow and Combustion in a Single Element GCH4/Gox Rocket Combustor: Chemistry Modeling and Turbulence-Combustion Interaction. In *52nd AIAA/SAE/ASEE Joint Propulsion Conference and Energy Forum: AIAA paper 2016-4996*, 2016.

[11] H. Müller, C. A. Niedermeier, J. Matheis, M. Pfitzner, and S. Hickel. Large-eddy simulation of nitrogen injection at trans- and supercritical conditions. *Physics of Fluids*, 28(1):015102–1–015102–28, 2016.

[12] N. Perakis, O. J. Haidn, D. Rahn, D. Eiringhaus, S. Zhang, Y. Daimon, S. Karl, and T. Horchler. Qualitative and quantitative comparison of rans simulation results for a 7 element gox/gch₄ rocket combustor. In *54th AIAA/SAE/ASEE Joint Propulsion Conference and Energy Forum: AIAA paper 2018-4556*, 2018.

[13] N. Peters. *Turbulent Combustion*. Cambridge University Press, Cambridge, 2000.

[14] B. E. Poling, J. M. Prausnitz, and J. P. O'Connell. *The properties of gases and liquids*. McGraw-Hill, New York, 2001.

[15] S. B. Pope. *Turbulent Flows*. Cambridge University Press, Cambridge, 2010.

[16] D. Preclik, G. Hagemann, O. Knab, C. Mäding, D. Haeseler, O. Haidn, A. Woschnak, and M. DeRosa. LOx/Hydrocarbon Preparatory Thrust Chamber Technology Activities in Germany. In *Proceedings of the 41st AIAA/ASME/SAE/ASEE Joint Propulsion Conference & Exhibit, Tucson, Arizona*, 2005.

[17] D. Rahn, H. Riedmann, R. Behr, and O. J. Haidn. Non-adiabatic flamelet modeling for the numerical simulation of methane combustion in rocket thrust chambers. In *54th AIAA/SAE/ASEE Joint Propulsion Conference and Energy Forum: AIAA paper 2018-4869*, 2018.

[18] R. Ranjan, A. Panchal, and S. Menon. On the Effects of Chemical Kinetics and Thermal Conditions on the Flow and Flame Features in a Single-Element GCH4/GOx Rocket Combustor. In *52nd AIAA/SAE/ASEE Joint Propulsion Conference and Energy Forum: AIAA paper 2016-4999*, 2016.

[19] R. C. Reid, J. M. Prausnitz, and B. E. Poling. *The Properties of Liquids and Gases*. McGraw-Hill, New York, 1987.

[20] S. Silvestri, M. P. Celano, G. Schlieben, and O. J. Haidn. Characterization of a Multi-Injector GOx-GCH4 Combustion Chamber. In *52nd AIAA/SAE/ASEE Joint Propulsion Conference: AIAA paper 2013-4071*, 2016.

[21] G. Singla, P. Scouflaire, C. Rolon, and S. Candel. Transcritical Oxygen/Transcritical or Supercritical Methane Combustion. *Proceedings of the Combustion Institute*, 30(2):2921–2928, 2005.

[22] G. Soave. Equilibrium constants from a modified Redlich-Kwong equation of state. *Chemical Engineering Science*, 27:1197–1203, 1972.

[23] C. Traxinger, M. Banholzer, and M. Pfitzner. Real-gas effects and phase separation in underexpanded jets at engine-relevant conditions. In *2018 AIAA Aerospace Sciences Meeting*, page 1815, 2018.

[24] C. Traxinger, J. Zips, and M. Pfitzner. Single-Phase Instability in LOx-CH₄ and LOx-H₂ Flames Under Rocket Engine Relevant Conditions. *Journal of Propulsion and Power*, 2019.

[25] A. W. Vreman. An eddy-viscosity subgrid-scale model for turbulent shear flow: Algebraic theory and applications. *Physics of fluids*, 16(10):3670–3681, 2004.

[26] J. Zips, H. Müller, and M. Pfitzner. Efficient Thermo-Chemistry Tabulation for Non-Premixed Combustion at High-Pressure Conditions. *Flow, Turbulence and Combustion*, 101(3):821–850, 2018.

[27] J. Zips, C. Traxinger, P. Breda, and M. Pfitzner. LES of a 7-Element GOx/GCH₄ Subscale Combustion Chamber Using Presumed and Transported PDF Methods. *Journal of Propulsion and Power*, 2019.

[28] J. Zips, C. Traxinger, and M. Pfitzner. Time-Resolved Flow Field and Thermal Loads in a Single-Element GOx/GCH₄ Rocket Combustor. *International Journal of Heat and Mass Transfer*, 2019, Under review.

[29] S. Zurbach, J. L. Thomas, P. Vuillermoz, L. Vingert, and M. Habiballah. Recent Advances on LOx/Methane Combustion for Liquid Rocket Engine Injector. In *38th AIAA/ASME/SAE/ASEE Joint Propulsion Conference and Exhibit: AIAA paper 2002-4321*, 2002.